19th Brazilian Congress of Thermal Sciences and Engineering
November 06th-10th, 2022, Bento Gonçalves - RS - Brazil

ENC-2022-0340
PRELIMINARY DESIGN OF AN AEROSPACE VEHICLE USING AIRBREATHING PROPULSION SYSTEM FOR HYPERSONIC SPEED

Laura Carolina Monteiro dos Santos Rodrigues da Silva
Instituto Tecnológico de Aeronáutica/ITA. Programa de Pós-Graduação em Ciências e Tecnologias Espaciais. Praça Marechal Eduardo Gomes, 50 - Vila das Acácias, CEP 12228-900, São José dos Campos/SP, Brasil
lauracarolinamsr@gmail.com

Juan Pablo de Lima Costa Salazar
Eduardo de Carli da Silva
Universidade Federal de Santa Catarina/UFSC – Campus Joinville. Rua Dona Franscisca, 8300 – Zona Industrial Norte, CEP 89219-600, Joinville/SC, Brasil
juan.salazar@ufsc.br; e.carli@ufsc.br

George Santos Marinho
Universidade Federal do Rio Grande do Norte/UFRN – Escola de Ciências e Tecnologia. Programa de Pós-Graduação em Engenharia Aeroespacial. Av. Senador Salgado Filho, 3000 – Campus Universitário, Lagoa Nova, CEP 59078-970, Natal/RN, Brasil
gmarinho@ct.ufrn.br

Paulo Gilberto de Paula Toro
Universidade Federal do Rio Grande do Norte/UFRN – Escola de Ciências e Tecnologia. Programa de Pós-Graduação em Engenharia Aeroespacial. Av. Senador Salgado Filho, 3000 – Campus Universitário, Lagoa Nova, CEP 59078-970, Natal/RN, Brasil

Instituto Tecnológico de Aeronáutica/ITA. Programa de Pós-Graduação em Ciências e Tecnologias Espaciais. Praça Marechal Eduardo Gomes, 50 - Vila das Acácias, CEP 12228-900, São José dos Campos/SP, Brasil
toro11pt@gmail.com

Abstract. *A low-cost design tool was developed, implemented and applied to the preliminary design of an aerospace vehicle using a hypersonic airbreathing propulsion system, based on supersonic combustion (scramjet) technology. A theoretical-analytical approach was used to determine the geometry for the scramjet vehicle. Hypotheses of quasi one-dimensional, steady, and inviscid flow were considered, and the fluid was treated as a calorically perfect gas. The scramjet model was divided into a compression section, a combustor, and an expansion section. In the compression section, oblique shock wave theory was applied. One-dimensional flow with heat addition (Rayleigh) theory was applied in the combustor. Finally, in the expansion section, area ratio theory was applied coupled with the expansion wave (Prandtl-Meyer) theory. In order to implement the developed tool, a scramjet operating at 25 km and Mach number 6.5 was considered. The scramjet vehicle geometry was obtained, including the compression ramp angles and expansion ramp angle. Also, the flow thermodynamic properties and flow Mach number are presented. Other geometries can be obtained by changing geometric parameters or operational parameters, such as altitude and flight speed. The preliminary geometry design can serve as a starting point for future studies using computational fluid dynamics (CFD) and experimental investigations.*

Keywords: *Supersonic Combustion, Hypersonic Airbreathing Propulsion, Scramjet, Hypersonics.*

1. INTRODUCTION

The aerospace science sector constantly seeks the development of new technologies in order to reduce the size, weight and energy consumption of launch vehicles. However, current systems, rocket engines, indicate little possibility of improvement through weight reduction, since they already have high efficiency.

In this context, the technology of hypersonic airbreathing propulsion systems with supersonic combustion (scramjet) presents itself as a tentative solution for the aerospace sector, since it can fulfill the requirements of high performance and reliability, as well as the limitations of fuel transport, as it uses atmospheric air as the oxidant. With no need to

carry the oxidant, unlike current rocket engines, the total weight of the vehicle is reduced, which implies a smaller amount of fuel needed and a smaller vehicle, resulting in a significant reduction in costs.

According to Heiser and Pratt (1994), ramjets are engines that do not have moving parts, which means they do not have rotating components. Ramjets are designed to operate in a speed range of Mach number 3 to 6, and their operation is based on the Brayton cycle. In this case, the vehicle surfaces are responsible for compressing the flow through oblique shock waves, ending with a normal shock wave, so that the flow reaches subsonic velocity in the combustion chamber. When the flow presents a Mach number greater than 6, considering ramjets, the process of decelerating it causes very high pressures and temperatures in the combustion chamber, which results in the decomposition of the air molecules, without combustion. At this operating speed the engine becomes a drag device.

In order to avoid this problem, compression is performed exclusively through oblique shock waves, and the flow is supersonic throughout the device. In this case, the airbreathing propulsion system is known as a supersonic combustion ramjet - scramjet, which presents better performance for flights with Mach numbers above 6 (Curran, 2001).

Figure 1 and Table 1 presents the common terminology and description for the main features of scramjet vehicles, according to Heiser and Pratt (1994).

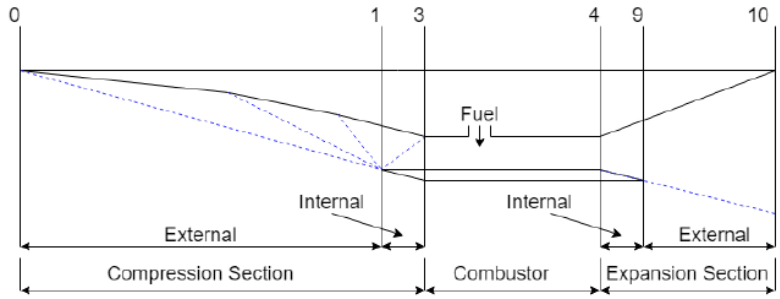

Figure 1. Schematic of scramjet system, adapted from Heiser and Pratt (1994).

Table 1. Description of the terminology for the scramjet vehicle, adapted from Heiser and Pratt (1994).

Station	Description
0	Scramjet vehicle leading-edge
1	Cowl leading-edge
3	Combustion chamber inlet
4	Combustion chamber exit
9	Cowl trailing-edge
10	Scramjet vehicle trailing-edge

This technology is still a matter of research, therefore it is necessary to survey the requirements and needs for the design, in order to assess possible challenges. In this way, the motivation is the simplified analysis and the implementation of simple and concise methodologies for the development of vehicles using hypersonic airbreathing propulsion, in order to determine more favorable configurations for future studies.

2. METHODOLOGY

In order to determine the geometry of the scramjet vehicle for a given geometric altitude and a given Mach number, it is first necessary to determine the sections to be dimensioned. Following the nomenclature given by Heiser and Pratt (1994) presented in Fig. 1, the scramjet vehicle is divided into three sections: compression section, combustor and expansion section.

2.1 Compression section

For the design of the compression section, the oblique shock wave theory is applied, in order to ensure that the freestream airflow is compressed and achieves the thermodynamic air properties and airflow velocity at the combustion chamber necessary for supersonic combustion and generation of thrust, as the vehicle reaches higher flight velocity.

According to Anderson (2003), oblique shocks occur when the supersonic or hypersonic flow is deflected with respect to the direction of incoming flow. Thus, when faced a wedge with a deflection angle θ, the flow is forced to change its direction abruptly, remaining parallel to the surface. In the frontal region of the wedge, an oblique shock wave is established, as shown in Fig. 2.

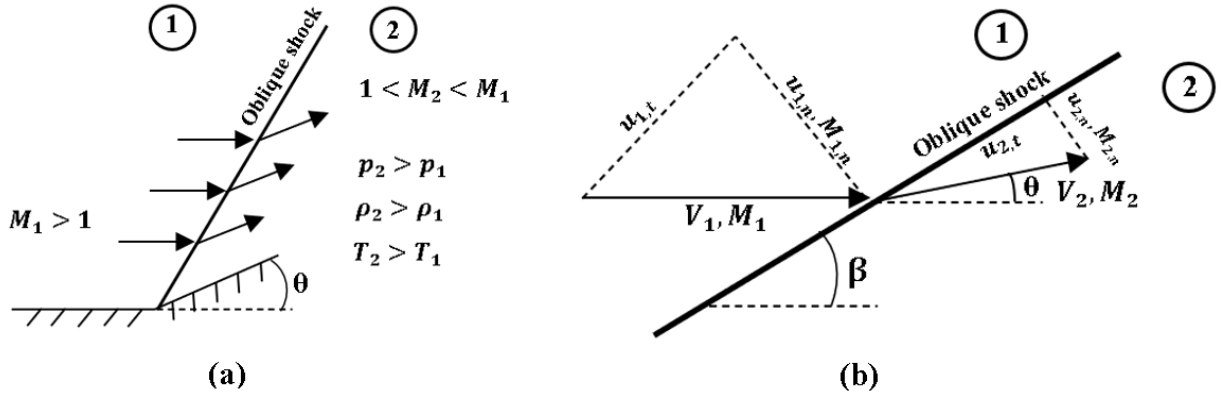

Figure 2. Oblique shock wave analysis, adapted from Anderson (2003).

Considering the simplifications of one-dimensional flow, stationary, adiabatic and inviscid flow, disregarding body forces and considering a calorically perfect gas, the equations of continuity, momentum and energy lead to a set of algebraic equations that relate gas properties after and before the oblique shock (Anderson, 2003). From the configuration shown in Fig. 2b, the following relations can be deduced:

$$M_{1,n} = M_1 \sin\beta \tag{1}$$

$$\frac{p_2}{p_1} = 1 + \frac{2\gamma}{\gamma+1}\left(M_{1,n}^2 - 1\right) \tag{2}$$

$$\frac{\rho_2}{\rho_1} = \frac{(\gamma+1)M_{1,n}^2}{(\gamma-1)M_{1,n}^2 + 2} \tag{3}$$

$$\frac{T_2}{T_1} = \frac{p_2}{p_1}\frac{\rho_1}{\rho_2} \tag{4}$$

$$M_{2,n}^2 = \frac{M_{1,n}^2 + \left[2/(\gamma-1)\right]}{\left[2\gamma/(\gamma-1)\right]M_{1,n}^2 - 1} \tag{5}$$

$$M_2 = \frac{M_{2,n}}{\sin(\beta-\theta)} \tag{6}$$

where: M_1, M_2, $M_{1,n}$, $M_{2,n}$ are the Mach number before and after the oblique shock wave and normal components of the Mach number before and after the oblique shock wave, respectively. p_2/p_1, ρ_2/ρ_1 and T_2/T_1 are the pressure, density and temperature ratios through oblique shock wave. In the equations above, subindices 1 and 2 correspond to the properties before and after the oblique shock.

The relation between the surface angle θ, the oblique shock wave angle β and the Mach number of the incident shock wave M_1, known as the *θ-β-M* relation, is given by Eq. (7), where γ is the specific heat ratio (γ = 1.4, for calorically perfect air).

$$\tan\theta = 2\cot\beta\left[\frac{M_1^2\sin^2\beta - 1}{M_1^2(\gamma + \cos 2\beta) + 2}\right] \tag{7}$$

According to Anderson (2003), a reflected oblique shock results when an incident oblique shock meets a flat surface, with a reflection angle such that the flow direction remains parallel to the surface, as shown in Fig. 3.

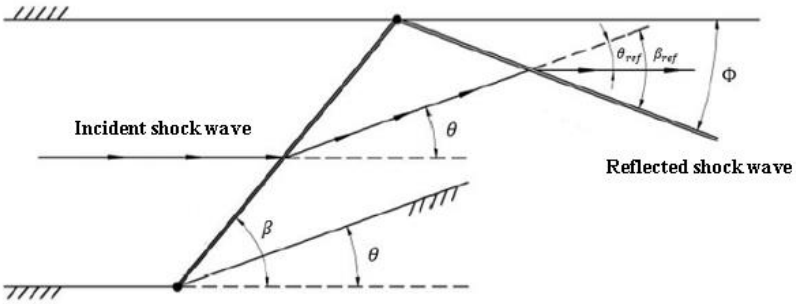

Figure 3. Reflected shock wave geometry (adapted from Anderson, 2003).

Based on the optimization criterion proposed by Oswatitsch (1947), and the methodology suggested by Ran and Mavris (2005) both applied to mixed supersonic inlet system, Carneiro (2020), Araújo et al. (2021) and Carneiro et al. (2022) modified this optimization criterion applying to the mixed hypersonic compression system.

The optimization criterion applied to a mixed supersonic inlet system (Oswatitsch, 1947; Ran and Mavris, 2005) results in a constant shock intensity through the mixed supersonic compression system with n-1 incident oblique shock waves, terminating with a normal shock, and subsonic speed at the combustion chamber entrance. For the mixed hypersonic compression system shown in Fig. 4, the intensity is constant through the incident oblique shock waves, and the last shock is a reflected oblique shock wave, which results in supersonic speed at the combustion chamber entrance (Carneiro, 2020; Araújo et al., 2021; Carneiro et al., 2022).

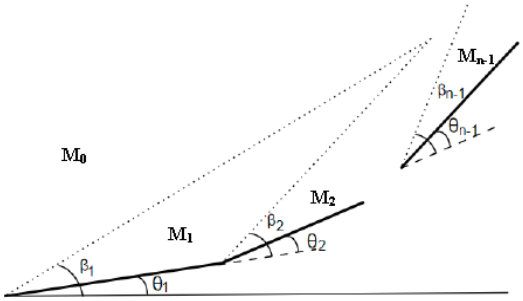

Figure 4. Schematic of mixed hypersonic compression system, adapted from Araújo et al. (2021).

Thus, considering the normal component of the oblique shock wave, the following equation for constant shock wave intensity is obtained, based on the configuration shown in Fig. 4.

$$M_0 \sin\beta_1 = M_1 \sin\beta_2 = \ldots = M_{n-2} \sin\beta_{n-1} \tag{8}$$

2.2 Combustor

It is required that the temperature at the combustion chamber inlet is sufficient to promote the autoignition of the fuel.

In order to calculate the required temperature T_3 of the air at the combustion chamber inlet, it is considered that the heat given up by the air at supersonic speed is equal to the heat absorbed by the fuel to raise its temperature to the ignition point (Araújo et al., 2021).

$$T_3 = \frac{\dot{m}^{fuel} c_p^{fuel}}{\dot{m}^{air} c_p^{air}} \left(T_{ign}^{fuel} - T_{inj}^{fuel} \right) + T_{ign}^{fuel} \tag{9}$$

From the temperature T_3, it is possible to calculate the Mach number M_3 at the combustion chamber inlet (Heiser and Pratt, 1994):

$$M_3 = \sqrt{\frac{2}{\gamma-1}\left\{\left[\frac{T_0}{T_3}\left(1+\frac{\gamma-1}{2}M_0^2\right)\right]-1\right\}} \tag{10}$$

where the subindices 0 and 3 correspond to the stations shown in Fig. 1 and Tab. 1. $\dot{m}$ is the mass flow rate, c_p corresponds to the specific heat at constant pressure, and T_{ign} and T_{inj} are the ignition and injection temperatures of the fuel, respectively.

Temperature T_3 and Mach number M_3 are achieved by correctly setting the ramp angles and positions in the compression section.

In this preliminary methodology, the addition of fuel mass is disregarded and combustion is modeled by one-dimensional flow with heat addition theory (Rayleigh Flow). Knowledge of the properties at the combustion chamber inlet and the requirement that the flow must remain supersonic throughout the combustor, it is possible to determine the properties at the exit of the chamber from the following equations (Anderson, 2003):

$$\frac{p_4}{p_3} = \frac{1+\gamma M_3^2}{1+\gamma M_4^2} \tag{11}$$

$$\frac{T_4}{T_3} = \left(\frac{1+\gamma M_3^2}{1+\gamma M_4^2}\right)^2\left(\frac{M_4}{M_3}\right)^2 \tag{12}$$

$$\frac{\rho_4}{\rho_3} = \left(\frac{1+\gamma M_3^2}{1+\gamma M_4^2}\right)\left(\frac{M_3}{M_4}\right)^2 \tag{13}$$

where subindices 3 and 4 correspond to the stations shown in Fig. 1 and Tab. 1.

2.3 Expansion section

According to Heiser and Pratt (1994), the expansion system is responsible for efficiently accelerating the combustion products from the combustion chamber exit, which implies a minimal increase in the entropy of the system.

The expansion section is divided into two-parts. In the first part, an expansion wave occurs when the inviscid, adiabatic supersonic flow encounters an increase in section area due to a negative deflection ($\theta < 0$). In this case, an isentropic expansion fan is established, delimited by the angles μ_1 e μ_2, referring to the front and tail of the expansion wave, respectively, as show in Fig. 5 (Anderson, 2003).

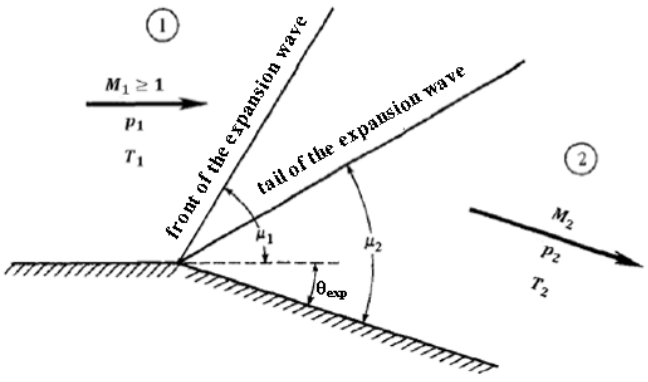

Figure 5. Prandtl-Meyer expansion wave, adapted from Anderson (2003).

According to Anderson (2003), the Prandtl-Meyer expansion theory considers that the angle of expansion θ_{exp} is given by:

$$\theta_{\exp} = \nu(M_2) - \nu(M_1) \tag{14}$$

where *ν(M)* is the Prandtl-Meyer function, given by:

$$\nu(M) = \sqrt{\frac{\gamma+1}{\gamma-1}}\tan^{-1}\left(\sqrt{\frac{\gamma-1}{\gamma+1}\left[M^2-1\right]}\right) - \tan^{-1}\left(\sqrt{M^2-1}\right) \tag{15}$$

Furthermore, μ_1 and μ_2 are the Mach wave angles, at the front and tail of the expansion wave, calculated by:

$$\mu = \sin^{-1}\frac{1}{M} \tag{16}$$

Once the Mach number after the expansion wave is known, it is possible to obtain the thermodynamic properties of the flow using the isentropic relations presented by Anderson (2003).

The Prandtl-Meyer expansion theory is valid only in the region bounded by the expansion wave front and its reflections, shown in Fig. 6. After this region, the area ratio theory presented by Anderson (2003) is applied. In this theory, the thermodynamic properties of the flow vary according to the change in the cross-sectional area of the flow. A quasi-one-dimensional flow is considered, where the properties vary only as a function of the position in the main flow direction, and the area *A* also varies as a function of position (Anderson, 2003). At each section, uniform properties are assumed.

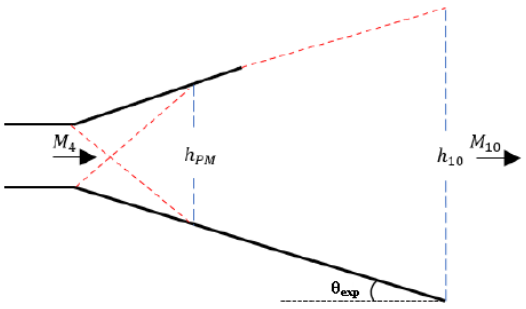

Figure 6. Schematic of expansion section.

3. COMPUTATIONAL MODELING

A low-cost computational tool was developed in Matlab, capable of obtaining the scramjet geometry, considering three subsystems: compression section, combustor, and expansion section. Below the main features of this tool are described.

Flight speed and flight altitude are the input parameters required to determine vehicle geometry. In order to calculate the thermodynamic properties of freestream flow, the atmospheric model of the US Standard Atmosphere (1976) was adopted.

With the input of a pre-defined number of ramps and initial estimate for the angle of the first ramp, the thermodynamic properties of the flow after the first oblique shock wave are calculated. Using the theory of constant shock wave intensity, the angles of the following ramps are determined, as well as the properties of the flow after each oblique shock. Then, the properties after the reflected shock wave are calculated, in order to determine the properties at the combustor inlet. If the properties obtained are different from those necessary for the autoignition of the fuel, in this case hydrogen, there is an increment in the value of the angle of the first ramp and the process is repeated until the desired configuration is found. The length of the ramps is defined in order to guarantee the occurrence of shock on-lip and shock on-corner.

In the combustion chamber, the theory of one-dimensional flow with heat addition (Rayleigh Flow) is applied, considering that the Mach number along the combustion chamber must remain supersonic.

Finally, for the expansion section, the Prandtl-Meyer expansion theory coupled to the area ratio theory is applied, considering a perfectly expanded flow at the exit, that is, the pressure at the exit must be equal to the freestream flow pressure.

Figure 7 shows the flow chart of the main algorithm.

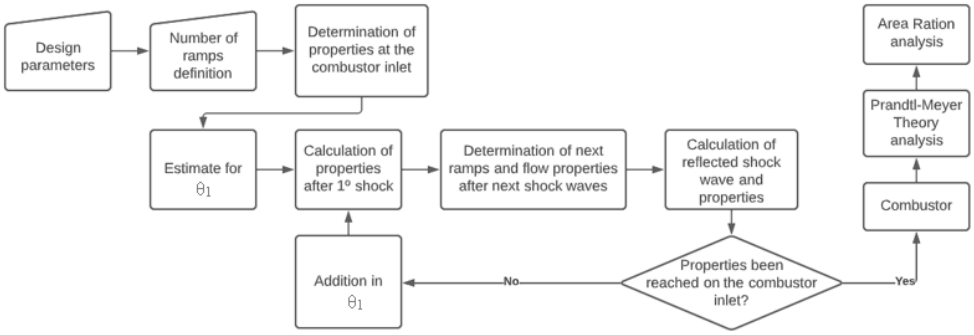

Figure 7. Schematic of scramjet preliminary design tool.

The adopted geometric limitations are based on the vehicle used to accelerate the scramjet vehicle to the operating speed. Figure 8 shows the geometry of the scramjet vehicle and Tab. 2 gives their dimensions.

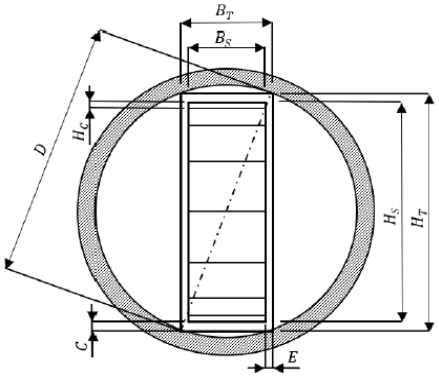

Figure 8. Representation of scramjet vehicle positioning, from Carneiro (2020).

Table 2. Scramjet engine coupling dimensions, from Carneiro (2020).

	Description	**Dimension [mm]**
B_S	Inlet width	102.8
B_T	Vehicle width	122.8
C	Cowl thickness	15
D	Internal diameter	428
E	Vehicle side thickness	10
H_C	Height of the combustion chamber	-
H_S	Inlet height	380
H_T	Vehicle height	410

4. RESULTS AND DISCUSSION

In order to demonstrate the use of the modeling strategy, a case study was chosen, considering the flight altitude of 25 km and flight speed of 1879.85 m/s, equivalent to Mach number 6.3.

The thermodynamic properties of the flow at the geometric altitude of 25 km are shown in Tab. 3.

Table 3. Freestream properties at 25 km geometric altitude.

Geometric altitude (Z) [km]	**Temperature (T) [K]**	**Pression (p) [Pa]**	**Density (ρ) [kg/m³]**	**Speed of sound (a) [m/s]**
25	221.55	2549.22	0.04008	298.39

The number of ramps adopted in this study was determined based on Martos (2017), who analyses the relation between the number of ramps and the compression efficiency and affirms that three ramps in the compression section guarantees the ideal balance between efficiency and complexity. The temperature T_3 and Mach number M_3 at the combustor inlet are calculated, according to Eqs. (9) and (10), in order to ensure that the hydrogen reaches the

autoignition temperature of 845.15 K, according to CRC (1983), considering that it is initially at a temperature of 300 K.

Table 4. Combustor inlet requirements

Fuel	Ignition temperature (T_{ign}) [K]	Injection temperature (T_{inj}) [K]	Combustor inlet	
			Mach	Temperature (T_3) [K]
Hydrogen	845.15	300	2.06	1017.25

In order to analyze the effect of combustion on the geometry of the expansion section, two cases were analyzed: power-off and power-on. In the first case, power-off, heat addition was not considered, so the properties at the combustor inlet and exit remain the same. In the second case, power-on, heat addition was considered according to section 2.2.

From the developed computational tool and considering the geometric factors presented, the following results are obtained for the geometry of the scramjet vehicle under study, presented in Tab. 5. For the compression section, the incident and reflected oblique shock wave theory was used, while for the expansion section, Prandtl-Meyer expansion and area ratio were considered. Two different angles were obtained for the expansion section of the power-on and power-off conditions, resulting in two different total lengths.

Table 5. Vehicle geometric results.

	Ramp 1	Ramp 2	Ramp 3	Reflection (combustor)	Expansion (power-on)	Expansion (power-off)	Total (power-on)	Total (power-off)
θ [°]	6.822	8.099	9.692	24.614	31.090	13.03	-	-
β [°]	14.248	17.0388	20.628	39.650	-	-	-	-
Length [mm]	436.83	189.21	165.32	(500.00)	295.84	770.98	1587.20	2062.34

The thermodynamic properties along the geometry for the scramjet vehicle for the condition power-on are presented in Tab. 6. It is important to notice that the criterion that determined the minimum required temperature of 1071.25 K at the entrance of the combustor was reached, which ensures that the fuel is self-ignited. Furthermore, a perfect expansion regime was obtained, since the pressure at the exit of the expansion section is equal to the freestream pressure.

Table 6 also presents the ratios for the thermodynamic properties. It is possible to notice that the ratio of the thermodynamic properties remains constant for the three ramps of the external compression section, which occurs because of the constant intensity of the incident oblique shock waves. An increase in the pressure ratio due to the existence of the reflected oblique shock wave is seen, causing a substantial increase in pressure compared to the incident oblique shock waves.

According to Tab. 6, the compression section results in a reduction in flight speed and Mach number and an increase in the thermodynamic properties of the flow. Thermodynamic properties decrease in the expansion section, while Mach number and speed increase. Additionally, the increase in thermodynamic properties occurs more abruptly after the reflected shock, when compared to the incident shocks.

Table 6. Results of thermodynamic properties along the scramjet engine.

	M [-]	p [Pa]	T [K]	ρ [kg/m³]	a [m/s]	V [m/s]	p_{n+1}/p_n	ρ_{n+1}/ρ_n	T_{n+1}/T_n
Freestream	6.3	2549.22	221.55	0.0401	298.39	1879.85	-	-	-
Ramp 1	5.29	6725.48	300.02	0.0781	347.23	1837.44	2.6382	1.9483	1.3542
Ramp 2	4.40	17743.50	406.27	0.1522	404.07	1778.39	2.6382	1.9483	1.3542
Ramp 3	3.60	43811.84	550.16	0.2964	470.21	1695.16	2.6382	1.9483	1.3542
Combustor inlet	2.06	281206.48	1071.25	0.9145	656.13	1351.47	6.0072	3.0851	1.9472
Combustor exit	1.25	612227.07	1870.05	1.1405	866.90	1083.63	2.1771	1.7457	1.2472
Expansion section (Prandtl-Meyer)	2.37	114350.56	1157.87	0.3440	682.14	1617.09	0.1868	0.6182	0.3017
Expansion section (area ratio)	5.14	2549.22	390.58	0.0227	396.18	2036.64	0.0223	0.3373	0.0661

From the thermodynamic properties at the exit of vehicle, presented in Tab. 6, the velocity of the combustion products is 2036.64 m/s, which is higher than the flight speed of 1879.85 m/s. This implies the capacity to generate thrust.

Figure 9 compares the thermodynamic properties and flight speed for power-on and power-off conditions.

The curves for the power-on and power-off conditions present similar behavior. However, for the power-on condition, the flight speed in the expansion section shows a significant increase with respect to the combustor and it is higher when compared to the curve for the power-off condition.

With the heat addition in the combustor, the temperature for the power-on condition is higher than the power-off condition. In the expansion section, the curves overlap. However, the final temperature of the power-on condition remains higher than the power-off condition.

Density and pressure show curves with similar behavior in the expansion section for the power-on and power-off cases. However, the curves for the power-off condition are higher than the power-on condition, despite the lower value in the combustor, due to the difference in the angle of the expansion section.

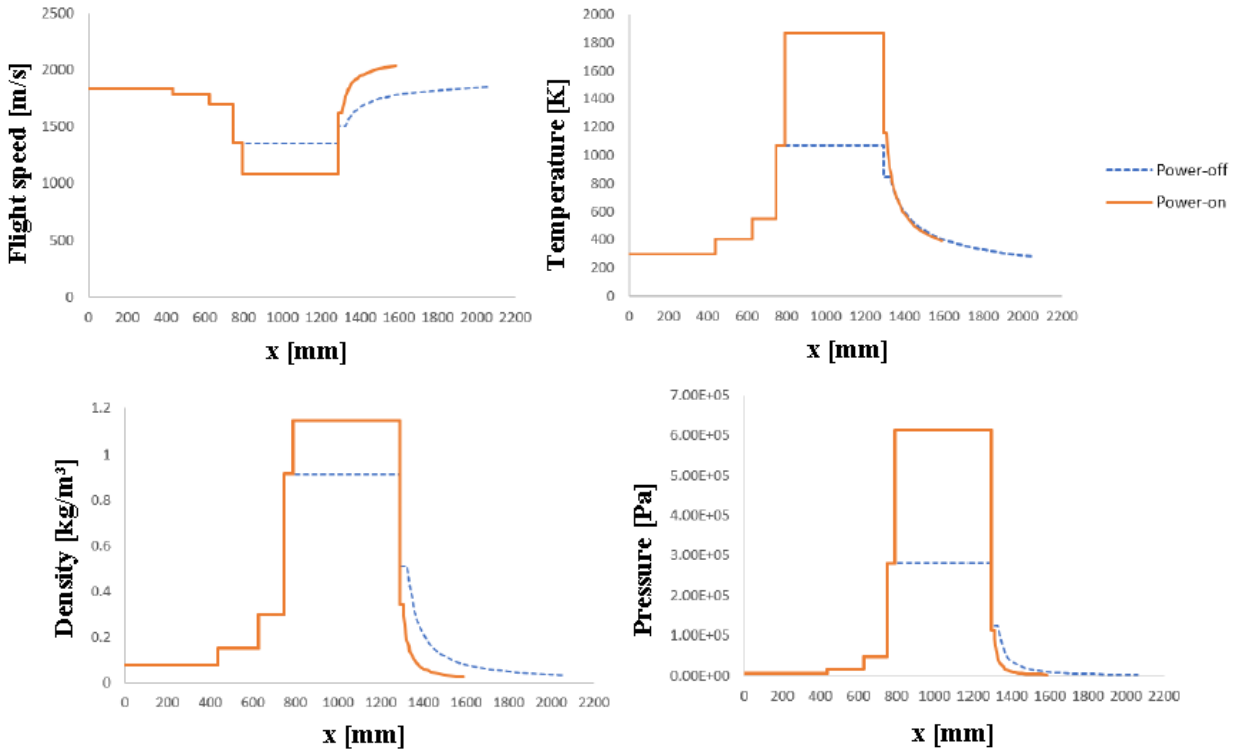

Figure 9. Thermodynamic properties and flight speed behavior under power-on and power-off conditions.

5. CONCLUSION

A preliminary design tool for hypersonic airbreathing vehicles based on supersonic combustion (scramjet) was developed. The analysis of the project was divided according to the vehicle systems: compression section, combustor and expansion section. In order to simplify the flow analysis and facilitate the preliminary design of the scramjet vehicle, atmospheric air was considered as calorically perfect gas, which implies a constant value for γ. In addition, inviscid flow was considered. The angles obtained for the compression ramps guarantee maximum air capture and constant shock wave intensity, in addition to ensuring that the temperature at the combustor inlet is sufficient for the fuel to self-ignite.

A preliminary design of a scramjet vehicle was developed to operate at 25 km altitude at a speed flight of 1879.85 m/s, corresponding to Mach number 6.3. Two geometries were generated, for power-on and power-off conditions. Both geometries met the design requirement of minimum temperature of 1071.25 K at the combustor inlet and both cases present the occurrence of shock on-lip and shock on-corner. From the configuration of the expansion section, it was possible to obtain a perfectly expanded flow at the nozzle exit, since the pressure was equal to the freestream pressure.

Results show that the design condition interferes with the geometry of the vehicle. Thus, the addition of heat in the combustor results in an increase in the angle of the ramp of the expansion section and a consequent reduction in the length of the vehicle. It is necessary to evaluate preliminary geometries across the entire operating range in order to achieve a good preliminary configuration.

This work aimed at an introductory study of the design of scramjet vehicles. A more accurate analysis of the expansion section requires the use of the method of characteristics or other computational fluid dynamics approaches. However, the objective of this work was to present a simplified methodology capable of guiding the project in a

preliminary design stage. Later steps should investigate boundary layer effects and high temperature effects such dissociation, as well as include the combustion process in detail, as this is a critical part of scramjet engine operation. From a more elaborate analysis, a different positioning of the ramps in the compression section is expected, as well as a new length for the combustor that guarantees the occurrence of the combustion process, in addition to guaranteeing the correct calculation of the mass flow.

6. ACKNOWLEDGEMENTS

This study was financed in in part by the Coordenação de Aperfeiçoamento de Pessoal de Nível Superior - Brasil (CAPES) - Finance Code 001. This work was carried out with the support of the Academic Cooperation Program in National Defense (PROCAD-DEFESA), grant 88887.387752/2019-00. The authors would like to thank the Instituto Tecnológico de Aeronáutica (ITA), Universidade Federal de Santa Catarina (UFSC) e Universidade Federal do Rio Grande do Norte (UFRN).

7. REFERENCES

Anderson, J.D., 2003. Modern compressible flow: with historical perspective. McGraw-Hill Education.

Araújo, P. P. B.; Pereira, M. V. S.; Marinho, G. S.; Martos, J. F. A.; Toro, P. G. P., 2021. Optimization of scramjet inlet based on temperature and Mach number of supersonic combustion. Aerospace Science and Technology 116, 106864, 2021.

Atmosphere, U.S., 1976. NASA TM-X 74335.

Carneiro, R.; Araújo, P. P. B; Marinho, G. S.; Martos, J. F. A.; Passaro, A.; Toro, P. G. P., 2022. Leading-to-trailing edge theoretical design of a generic scramjet. AIP Advances 12, 055322 (2022).

Carneiro, R., 2020. Estudo analítico de um demonstrador da tecnologia da combustão supersônica. Master in mecanic engineering, Universidade Federal do Rio Grande do Norte, Natal.

CRC, Aviation Fuel Properties, 1983. Report 530, Coordinating Research Council, Inc.

Curran, E. T., 2001. Scramjet engines: the first forty years. Journal of Propulsion and Power, Vol. 17, No. 6, pp. 1138-1148.

Heiser, W. H. and Pratt, D. T., 1994. Hypersonic airbreathing propulsion. Washington, D. C., American Institute of Aeronautics and Astronautics.

Martos, J., 2017. Aerothermodynamic design, manufacture and testing of a 3-D prototyped scramjet. Doctor in science in the program of space science and technology, area of space propulsion and hypersonics, Instituto Tecnológico de Aeronáutica, São José dos Campos.

Oswatitsch, K., 1947. Pressure recovery for missiles with reation propulsion at high supersonic speeds (the effiency of shock diffusers). NACA Techinical Memorandum, Vol. 1140.

Ran, H. and Mavris, D., 2005. Preliminary design of a 2-D supersonic inlet to maximize total pressure recovery. AIAA 5th Aviation, Technology, Integration, and Operations Conference (ATIO), p. 11.

8. RESPONSIBILITY NOTICE

The authors are the only responsible for the printed material included in this paper.